Memoirs of the Faculty of Engineering, Nagoya University
Vol. 41, No. 1 (1989) —Research Report—

PROPAGATION MECHANISM OF DETONATION — THREE-DIMENSIONAL PHENOMENA

TOSHI FUJIWARA and K. VISWANATH REDDY

Department of Aeronautical Engineering

(Received May 31, 1989)

Abstract

A numerical technique has been applied, for the first time, to a three-dimentional detonation propagating in a tube of circular cross section. Using a million grid points on a supercomputer, the results have provided the mechanism of propagation; essentially the coupling among three different modes of shock waves, (i) the frontal wave in axial direction, (ii) the radial wave and (iii) the azimuthal waves. In particular, the azimuthal waves are always paired and flapping to one another to sustain the strength for self-propagation until there exists only one azimuthal wave in a so-called single-spinning mode.

Another conspicuous feature is the existence of fine structure in a triple shock intersection; multiple Mach reflections existing in a macroscopic triple point. Sometimes the number of Mach reflections amounts to 5 or 6.

A number of aspects found not only in two-dimensional unsteady detonations but also specific in three-dimensional detonations are presented.

1. Introduction

Study of detonation phenomena has reached a new stage due to the progress in computational fluid dynamics and measurement techniques using lasers. In particular, the capability of imaging three-dimensional structures and behaviors of a fluid-dynamic phenomenon is within the reach of a number of scientists, either on supercomputers or on high-speed holography/image intensifiers.

If we want to numerically analyze 3-dimensional new aspects of a detonation, i.e., (i) non-symmetrical 3-dimensional nonsteady structures, (ii) complicated interaction of numerous three-dimensional triple-shock intersections, (iii) a possibility of observing and clarifying the physics of a spinning head (what is spinning in the first place, and next what is the mechanism supporting the spin phenomenon ?), (iv) the irregular structure of leading frontal shock wave and its relation to the soot patterns recorded on the tube surface, and

(v) the mechanism of pulsating propagation velocity around the Chapman-Jouguet value, an extremely meticulous numerical diagnosis is necessary to provide all the informations on a typical detonation. In other words, a detonation has to be modeled as close to the reality as possible and should propagate for a distance long enough to give stationary (close-to-periodical) behaviors rather than transient ones that are sometimes misleading.

In order to make such a three-dimensional analysis feasible, it is vital to eliminate potential troubles generally encountered in the numerical analysis of a hypersonic reacting flow. They are usually (i) a flow containing very high and sharp discontinuities associated with strong shock waves, (ii) exothermic chemistry often containing tens of elementary chemical reactions, (iii) some stiffness problems related with several characteristic times of different order, and (iv) so-called the real gas effect representing the specific heat as a function of chemical species and temperature, (v) basic non-steadiness of the phenomenon, and (vi) complicated molecular diffusion among numerous chemical species.

2. Formulation of Problem

Here we try to eliminate the above-mentioned difficulties by introducing a modeling on the fluid dynamics and chemistry which has been successful in numerically providing detailed analyses of two-dimensional nonsteady phenomena, and upgrade the analyses to a three-dimensional nonsteady detonation propagating in a tube of circular cross section.

In order to avoid the stiffness and computing time problems, the complicated chemistry in an oxyhydrogen detonation is replaced by the Korobeinikov's two-step reaction model containing two dimensionless progress variable α and β ($0<\alpha, \beta<1$). The first one consists of an irreversible induction reaction generating no exothermicity, while the second one can give an equilibrium state between forward and backward reactions, accompanying heat generation in proportion to the change of the progress variable β, as shown in Eq. (6). In other words, the rates of mass production (mass/volume/time) of both species α and β are explicitly given by the following simple expressions:

(i) Induction Reaction;

$$W_\alpha \equiv \frac{d\alpha}{dt} = -\frac{1}{\tau_{ind}} = -K_1 \rho \exp\left(\frac{-E_1}{RT}\right). \tag{1}$$

(ii) Exothermic Reaction;

$$W_\beta \equiv \frac{d\beta}{dt} = \begin{cases} 0, & \alpha > 0, \\ -K_2 p^2 \left[\beta^2 \exp\left(\dfrac{-E_2}{RT}\right) - (1-\beta)^2 \exp\dfrac{-(E_2+Q)}{RT}\right], & \alpha \leq 0. \end{cases} \tag{2}$$

The detailed structure of this scheme can be explained as follows: First, due to the arrival of a strong shock wave, the chemical species α starts decreasing from 1 under the mass production rate (1), until it gets to 0 after an induction time of order τ_{ind}. Then β starts decreasing from 1 down to β_{eq} which is obtained by setting the right-hand-side of

Eq. (2) zero. The chemical parameters appearing in Eqs. (1) and (2) are selected to fit either $2H_2+O_2+7Ar$ or $2H_2+O_2+7He$ mixture at an initial pressure $P_0=0.1$ atm as:

$$\begin{aligned}&\text{Frequency factor; } K_1 = 3.0\times 10^{11} cm^3/g/sec.\\ &\text{Frequency factor; } K_2 = 1.5\times 10^{-7} cm^4/dyne^2/sec.\\ &\text{Activation energy; } E_1/R = 9{,}800K,\ E_2/R = 2{,}000K.\\ &\text{Heat of reaction; } Q = 4.0\times 10^{10} erg/g.\ R = gas\ constant.\end{aligned} \tag{3}$$

Even though this reaction model is much simpler than the real oxyhydrogen elementary reactions, it has been successful to give not only all the two-dimensional gasdynamic behaviors observed in a steadily-propagating detonation, but also to yield subtle phenomena like decoupling and quenching of a meta-stable plane ZND detonation by applying weak disturbances, or quenching and establishment of a detonation thrown out from a confined channel into a free space.

The fundamental gasdynamic equations are the Euler ones under the assumption of perfect gas (no real gas effects) and no transport phenomena. Real gas effects can give not only just reducing the temperature by allowing higher heat capacity as a result of molecular excitation of internal degrees of freedom, but also contribute to cause instability phenomena seen for example in a shock tube flow of large molecules. Nevertheless, they can be neglected in the present model from physics point of view, since already-existing chemical reactions play the role of such real gas effects. The importance of transport properties in detonation phenomena is getting recognized, particularly in detonation limits and in evaluating turbulence as a mechanism of ignition and energy supply to a detonation wave; in a turbulent flow, very fast vortical entrainement of cold unburnt mixture into hot reaction product and resulting prolonged contact between the two layers can trigger an explosion fast and strong enough to support a detonation wave traveling at about 2,000 m/sec without the presence of a frontal leading shock wave. This is a completely new concept to the theory of deflagration and detonation waves proposed by Lee. Verification of this possibility is one of the most interesting studies in the theory of detonation, which however is not accounted for in the present formulation. Thus, we have decided the Euler equations as our fundamental equations which are written in the following non-dimensional conservation-law form:

$$\frac{\partial V}{\partial t}+\frac{\partial E}{\partial x}+\frac{\partial F}{\partial y}+\frac{\partial G}{\partial z}+H=0, \tag{4}$$

where the inviscid flux vectors and the chemical source term vector are

$$V=\begin{vmatrix}\rho\\ \rho u\\ \rho v\\ \rho w\\ e\\ \rho\beta\\ \rho\alpha\end{vmatrix},\quad E=\begin{vmatrix}\rho u\\ \rho u^2+p\\ \rho uv\\ \rho uw\\ (e+p)u\\ \rho u\beta\\ \rho u\alpha\end{vmatrix},\quad F=\begin{vmatrix}\rho v\\ \rho vu\\ \rho v^2+p\\ \rho vw\\ (e+p)v\\ \rho v\beta\\ \rho v\alpha\end{vmatrix},$$

$$G=\begin{vmatrix}\rho w\\ \rho wu\\ \rho wv\\ \rho w^2+p\\ (e+p)w\\ \rho w\beta\\ \rho w\alpha\end{vmatrix},\quad H=\begin{vmatrix}0\\ 0\\ 0\\ 0\\ 0\\ -\rho W_\beta\\ -\rho W_\alpha\end{vmatrix}. \tag{5}$$

These equations can become a complete closed system by augmentation of the state equations

$$p=(\gamma-1)\left[e-\rho\beta Q-\frac{\rho(u^2+v^2+w^2)}{2}\right], \tag{6}$$

$$p=\rho RT. \tag{7}$$

Before solving the equations, the following non-dimensionalization is introduced:

(i) x, y are non-demensionalized by L^*, the induction length defined in the plane Chapman-Jouguet detonation;

$$L^*=0.0225/p_\infty(atm)\ \ cm \ \text{ for } \ 2H_2+O_2+7Ar. \tag{8}$$

(ii) The velocities u, v by α_∞ (sonic speed), the time t by L^*/α_∞, the internal energy e by $\rho_\infty\alpha^2{}_\infty$, the heat of reaction by $\alpha^2{}_\infty$, the temperature T by T_∞ and the density ρ by ρ_∞.

(9)

3. Numerical Scheme

As numerical scheme, the 2nd-order explicit MacCormack + the 4th-order FCT technique is utilized, because the method has been extremely successful in forming

non-oscillating and smooth shock wave profiles due to its TVD character; this is essential to a shock wave followed by highly temperature-sensitive exothermic chemical reactions. In other words, the method gives dependable stability in high-temperature reactions behind a strong shock wave.

The arbitrary coefficients contained in the 4th-order diffusion terms and FCT limiters are determined for the numerical results to provide physically plausible solutions; for example, automatic satisfaction of the Rankine-Hugoniot relations across the leading frontal shock wave, quenching character of two-dimensional detonations, and keeping the average propagation velocity at the Chapman-Jouguet value are used as criteria for judgment; thus the chosen values are

$$\mu_z=1.5/48,\ \mu_r=0.2/48,\ \mu_\varphi=0.1/48 \text{ and } \eta=0.7/8. \tag{10}$$

Because utilized is the $(z,\ r,\ \varphi)$ cylindrical coordinate system, the 4th-order diffusion terms in r direction are weighted in the following way, as pointed out by Book and others:

Predictor;

$$\begin{aligned} V^{(1)}_{i,j,k}=V^n_{i,j,k} &-\frac{\Delta t}{\Delta z}(E^n_{i+1,j,k}-E^n_{i,j,k})-\frac{\Delta t}{\Delta r}(F^n_{i,j+1,k}-F^n_{i,j,k}) \\ &-\frac{\Delta t}{\Delta \phi}(G^n_{i,j,k+1}-G^n_{i,j,k})-\Delta t H^n_{i,j,k}\ . \end{aligned} \tag{11}$$

Corrector;

$$\begin{aligned} \hat{V}^{n+1}_{i,j,k}=\frac{1}{2}\Bigg[\ V^n_{i,j,k}+V^{(1)}_{i,j,k} &-\frac{\Delta t}{\Delta z}(E^{(1)}_{i,j,k}-E^{(1)}_{i-1,j,k})-\frac{\Delta t}{\Delta r}(F^{(1)}_{i,j,k}-F^{(1)}_{i,j-1,k}) \\ &-\frac{\Delta t}{\Delta \phi}(G^{(1)}_{i,j,k}-G^{(1)}_{i,j,k-1})-\Delta t H^{(1)}_{i,j,k}\Bigg]\ . \end{aligned} \tag{12}$$

4th-Order Diffusion;

$$\begin{aligned} \tilde{V}^{n+1}_{i,j,k} =\hat{V}^{n+1}_{i,j,k} &-\mu_z(V^n_{i-2,j,k}-4V^n_{i-1,j,k}+6V^n_{i,j,k}-4V^n_{i+1,j,k}+V^n_{i+2,j,k}) \\ &-\mu_r(V^n_{i,j-2,k}-4V^n_{i,j-1,k}+6V^n_{i,j,k}-4V^n_{i,j+1,k}+V^n_{i,j+2,k}) \\ &-\mu_\phi(V^n_{i,j,k-2}-4V^n_{i,j,k-1}+6V^n_{i,j,k}-4V^n_{i,j,k+1}+V^n_{i,j,k+2}) \end{aligned} \tag{13}$$

FCT Limiters;

$$\overline{V}^{n+1}=\tilde{V}^{n+1}_{i,j,k}+\eta_z(V^n_{i+1,j,k}-2V^n_{i,j,k}+V^n_{i-1,j,k}). \tag{14}$$

$$\overline{\overline{V}}^{n+1}=\tilde{V}^{n+1}_{i,j,k}+\eta_r\left(\frac{r_{j+\frac{1}{2}}}{r_j}V^n_{i,j+\frac{1}{2},k}-\frac{r_{j-\frac{1}{2}}}{r_j}V^n_{i,j-\frac{1}{2},k}\right). \tag{15}$$

$$\tilde{\tilde{\tilde{V}}}^{n+1}_{i,j,k}=\tilde{V}^{n+1}_{i,j,k}+\eta_\phi(V^n_{i,j,k+1}-2V^n_{i,j,k}+V_{i,j,k-1}), \tag{16}$$

$$V^{n+1}_{i,j,k}=\overline{V}^{n+1}_{i,j,k}+\tilde{\tilde{V}}^{n+1}_{i,j,k}+\tilde{\tilde{\tilde{V}}}^{n+1}_{i,j,k}-2\tilde{V}^{n+1}_{i,j,k}-(\delta^c_{i+\frac{1}{2},j,k}-\delta^c_{i-\frac{1}{2},j,k}) -(\frac{r_{j+\frac{1}{2}}}{r_j}\delta^c_{i,j+\frac{1}{2},k}-\frac{r_{j-\frac{1}{2}}}{r_j}\delta^c_{i,j-\frac{1}{2},k})-(\delta^c_{i,j,k+\frac{1}{2}}-\delta^c_{i,j,k-\frac{1}{2}}), \tag{17}$$

where the coefficients are defined as

$$\delta^c_{i+\frac{1}{2},j,k}=S_1\cdot Max[0,\ Min(S_1,\ \Delta_{i-\frac{1}{2},j,k},|\tilde{\Delta}_{i+\frac{1}{2},j,k}|,S_1\cdot\Delta_{i+\frac{3}{2},j,k})], \tag{18}$$

$$\delta^c_{i,j+\frac{1}{2},k}=S_2\cdot Max[0,\ Min(S_2,\ \frac{r_j}{r_{j-\frac{1}{2}}}\Delta_{i,j-\frac{1}{2},k},|\tilde{\Delta}_{i,j+\frac{1}{2},k}|,S_2\cdot\frac{r_{j+1}}{r_{j+\frac{1}{2}}}\Delta_{i,j+\frac{3}{2},k})], \tag{19}$$

$$\delta^c_{i,j,k+\frac{1}{2}}=S_3\cdot Max[0,\ Min(S_3,\ \Delta_{i,j,k-\frac{1}{2}},|\tilde{\Delta}_{i,j,k+\frac{1}{2}}|,S_3\cdot\Delta_{i,j,k+\frac{3}{2}})], \tag{20}$$

$$\Delta_{i+\frac{1}{2},j,k}=\overline{V}^{n+1}_{i+1,j,k}-\overline{V}^{n+1}_{i,j,k}, \tag{21}$$

$$\Delta_{i,j+\frac{1}{2},k}=\tilde{\tilde{V}}^{n+1}_{i,j+1,k}-\tilde{\tilde{V}}^{n+1}_{i,j,k}, \tag{22}$$

$$\Delta_{i,j,k+\frac{1}{2}}=\tilde{\tilde{\tilde{V}}}^{n+1}_{i,j,k+1}-\tilde{\tilde{\tilde{V}}}^{n+1}_{i,j,k}, \tag{23}$$

$$\tilde{\Delta}_{i+\frac{1}{2},j,k}=\eta_z(\tilde{V}^{n+1}_{i+1,j,k}-\tilde{V}^{n+1}_{i,j,k}), \tag{24}$$

$$\tilde{\Delta}_{i,j+\frac{1}{2},k}=\eta_r(\tilde{V}^{n+1}_{i,j+1,k}-\tilde{V}^{n+1}_{i,j,k}), \tag{25}$$

$$\tilde{\Delta}_{i,j,k+\frac{1}{2}}=\eta_\phi(\tilde{V}^{n+1}_{i,j,k+1}-\tilde{V}^{n+1}_{i,j,k}), \tag{26}$$

$$S_1=sign(\tilde{\Delta}_{i+\frac{1}{2},j,k}),\quad S_2=sign(\tilde{\Delta}_{i,j+\frac{1}{2},k}),\quad S_3=sign(\tilde{\Delta}_{i,j,k+\frac{1}{2}}), \tag{27}$$

and

$$r_{j+\frac{1}{2}}=\frac{(r_j+r_{j+1})}{2}. \tag{28}$$

4. Results and Discussions

In order to avoid large errors arising from the mathematical singularity on the tube axis, we have placed a co-axial cylinder of radius r_i in the central part of the tube, as shown in Fig. 1 (a); thus, the detonation propagates between the outer and inner tubes of cylindrical symmetry. Two cases are considered; a "small tube" (outer radius $r_0=\frac{22L^*}{9}$ and inner radius $r_i=\frac{4L^*}{9}$ and the channel width $2L^*$) and a "large tube" (outer radius $r_0=\frac{46L^*}{9}$ and inner radius $r_i=\frac{10L^*}{9}$, the channel width $4L^*$). In each case, the total grids utilized are $450\times21\times110$ with uniform grid spacing $\frac{L^*}{9}$, and $350\times20\times126$ with $\frac{2L^*}{9}$, respectively, totaling about 1 million grids. Due to 100% vectorization, the speed of calculation is 15 times faster on FUJITSU VP-200 compared with a non-vector machine.

Initially we place a plane ZND detonation which is propagating at the Chapman-Jouguet Mach number in the above-mentioned co-axial cylinder. This detonation is

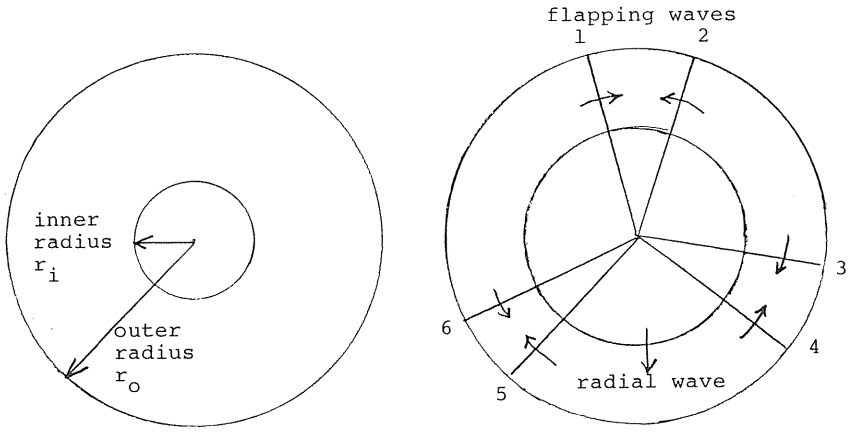

(a) Co-axial Tube.

(b) Two Wave Modes: Flapping and Radial.

Fig. 1. Tube geometry and the concept of "flapping" and "radial" waves propagating in the azimuthal and radial directions of tube cross section.

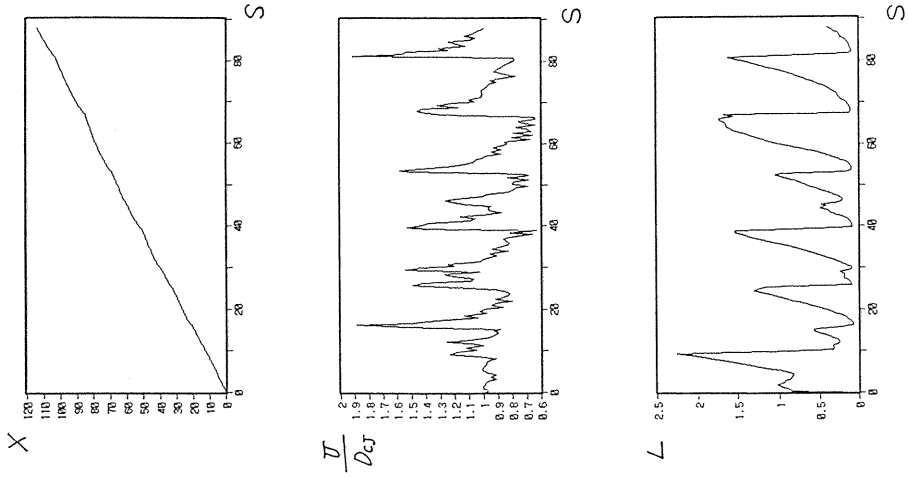

(a) (b) (c)

Fig. 2. An example of a two-dimensional detonation propagating in a channel of 6L* width. (a) x-t diagram of detonation front. (b) Axial propagation velocity of detonation on a wall as a function of Time Step S; fluctuating around the C-J value. (c) Chemical induction distance on a wall as a function of Time Step S.

numerically disturbed by placing one to several finite-size exothermicity spots in the path of the detonation front before it develops to have a complete structure of three dimensions.

4. 1. Detonation in a 2-Dimensional Channel:

An example of a two-dimensional detonation propagating in a channel is shown in Fig. 2. Although details of the structure and development from a plane ZND detonation are not given here, the following aspects are clearly observed:

(i) Average propagation velocity U is the Chapman-Jouguet value, as seen in (a), with strong fluctuations of amplitude between 0.65 and 1.9 observed in (b).
(ii) The fluctuation of U consists of two components, one with high amplitude and low frequency and the other with low amplitude and high frequency, as seen in (b). The former is caused by the collision of the transverse shock wave on the channel wall, whereas the latter by smaller-scale, more local and frequent explosions producing blast waves.
(iii) As a result of transverse shock wave collision, the temperature and pressure are temporarily augmented, yielding the behavior of the chemical induction time shown in (c). Note that the profiles of U and L perfectly correspond each other.

4. 2. Modes of Shock Wave:

The size, number, location and azimuthal direction of movement of the perturbations are changed to trigger conceivably different modes of wave propagation, such as single spinning, in 3-dimensional detonation. However, the results seem to show that the generated gas motion is essentially irrelevant to the type of trigger perturbations.

As seen in the schematic picture Fig. 1 (b), the two wave modes, flapping and radial, were observed in a tube cross section. Thus, it can be concluded that essentially three different modes of shocks (frontal flapping and radial) are interacting each other. Here the term "flapping" means that the waves propagating in the azimuthal direction are always paired and collide back and forth, just as a bird flaps its wings.

Due to complicated interactions among such three modes of shocks having different periodicities and phases of nearly periodical motion, it is usually very unlikely to obtain complete reproducibility in the observed physical quantities. Nevertheless, a detonation in a confined circular tube is strongly controlled by the geometry and therefore the phenomena are resonant and nearly periodical, where the frequencies of oscillation are the eigen values of the problem.

4. 3. Propagation Velocity of Detonation Front and Fluctuation:

Fig. 3 gives the propagation velocity of the detonation front at three different radii (outer wall surface, mid radius and inner wall surface) in typical 5 meridian planes (ϕ=0, 33.64, 235.51, 302.8 and 336.45 degrees). The calculation is for the smaller tube where the 5 meridian planes are typically picked up from the similar 110 planes with the interval 3.27 degree. When we see Fig. 3 (a), the propagation velocity on the outer wall (the top picture) is fairly reproducible with high and sharp peaks and less high-frequency components. On the other hand, the velocity on the outer wall in Fig. 3 (b) gives much lower peaks and more conspicuous low-amplitude high-frequency components. Similarity between (a) and (b) exists only on the inner wall, as far as the high-amplitude low-frequency components are concerned.

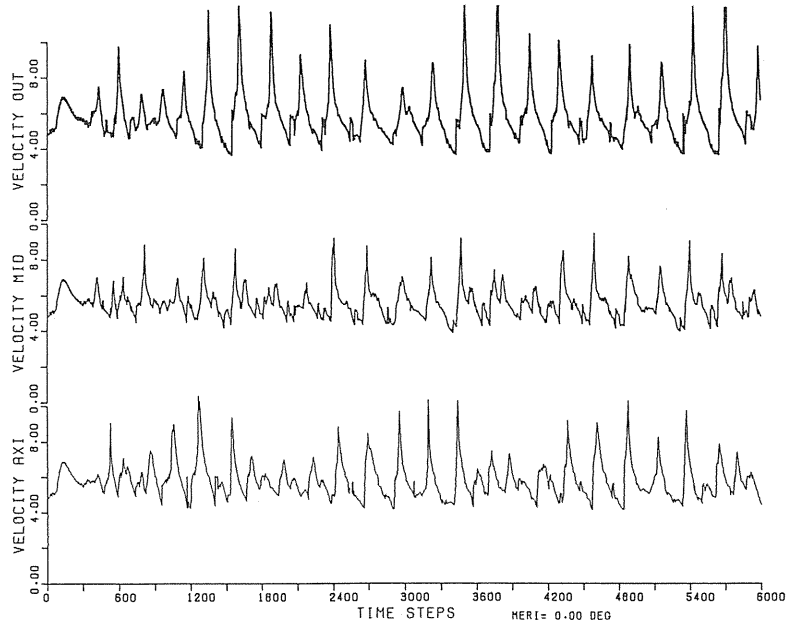

Fig. 3 (a) Propagation velocity of the detonation front at three different radii in the meridian plane ϕ=0 degree: A detonation in a tube of outer radius 22L*/9 and inner radius 4L*/9 at Time Step 5000. Total grids are $450 \times 21 \times 110$, based upon the uniform grid spacing L*/9, giving the azimuthal angle interval 3.36 degrees.

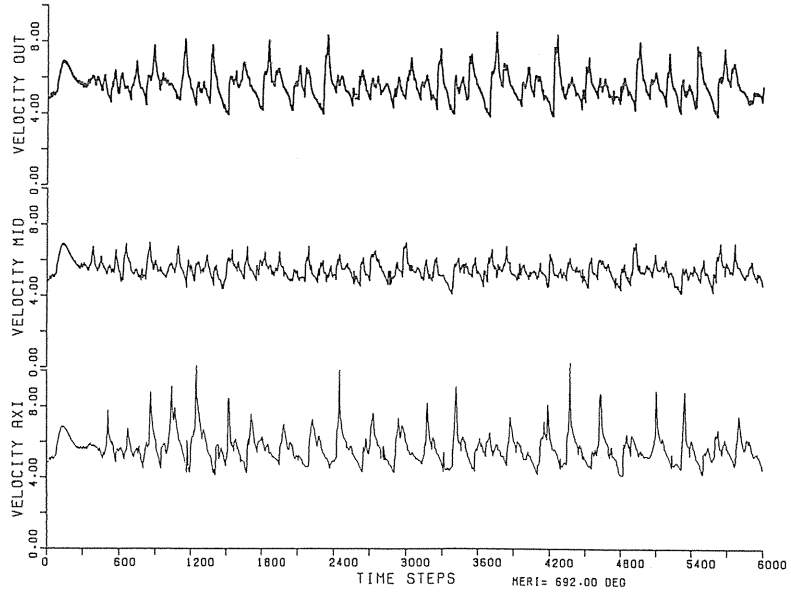

Fig. 3 (b) Propagation velocity of the detonation front at three different radii in the meridian plane ϕ=33.64 degree.

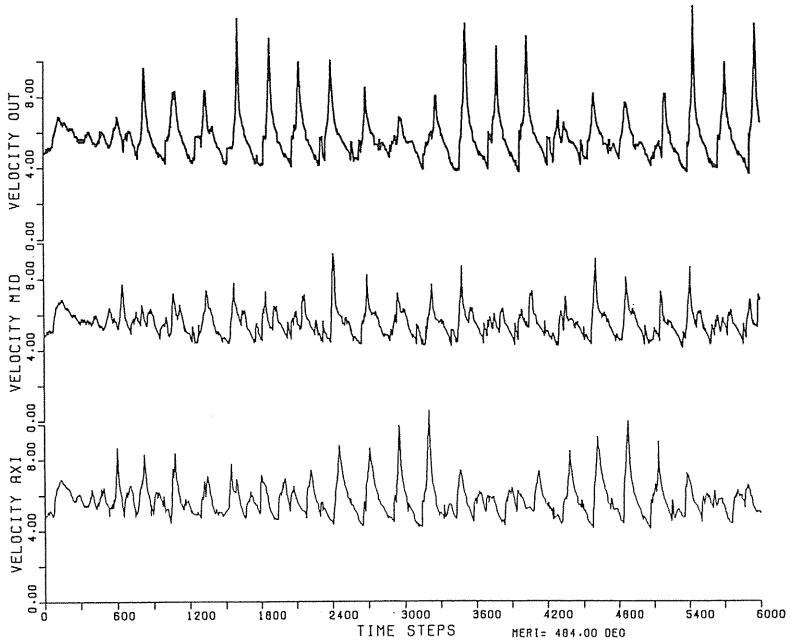

Fig. 3 (c) Propagation velocity of the detonation front at three different radii in the meridian plane ϕ=235.51 degree.

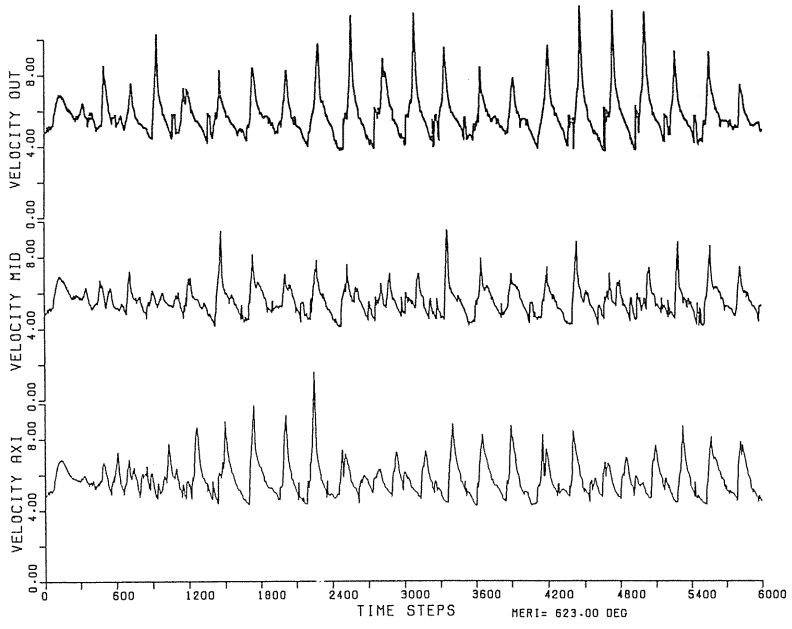

Fig. 3 (d) Propagation velocity of the detonation front at three different radii in the meridian plane ϕ=302.8 degree.

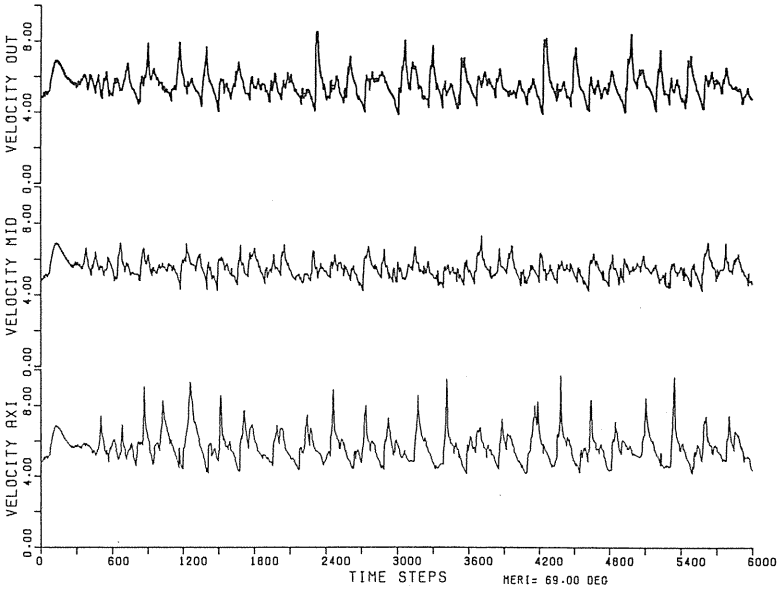

Fig. 3 (e) Propagation velocity of the detonation front at three different radii in the meridian plane ϕ=336.45 degree.

Interestingly, Figs.3 (c) and (d) are more or less similar to (a), because the high-amplitude low-frequency components are dominant in these meridian planes. In the similar fashion, Figs.(b) and (e) are alike each other as well, having less dominant low-frequency peaks superimposed with active high-frequency pulsations. Thus, the detonation phenomenon is different on different meridian planes where strong shock interaction occurs preferably on certain meridian planes. The shock waves arriving at the outer wall consists not only of conventional strong triple shock interactions but also of many other weaker shocks (still nonlinear) interacting each other.

The aspect is totally different from the two-dimensional counterpart where the primary pulsations are always caused by the arrival of triple points, being superimposed by higher-frequency nearly-acoustic pulsations of much smaller amplitudes. This indicates that when we observe only the strongest pulsation spinning azimuthally, if there is, among a few flapping shock waves in an extreme case, it would probably look like a single spinning head observed in the experiments.

Generally speaking, pulsating behaviors in one meridian plane are consistent; wave amplitudes are nearly alike. This shows that we have a nearly periodical motion. When a pair of flapping waves and a radial wave arrive on the outer wall at the same time, we would observe the highest pressure/velocity peak, whereas in other cases the peaks would be weaker depending upon the extent of simultaneousness.

4. 4. Pressure Distribution in Different Meridian Planes and Tube Cross Sections at a Given Time Step N = 5,000:

The frontal shock wave shape is far from planar, judging from the pressure distributions on the different meridian planes K = 18 − 33 in Fig.4 (a) and in the different tube

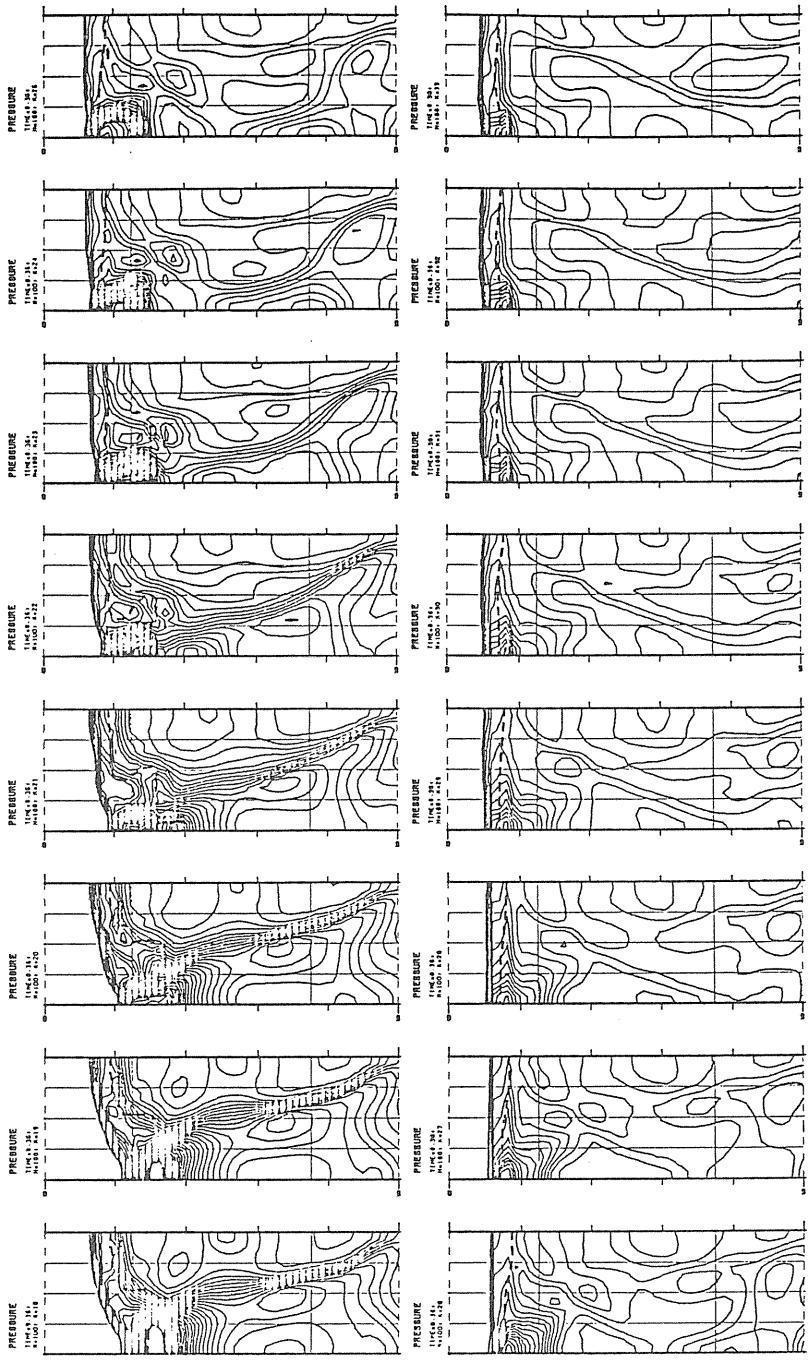

Fig. 4 (a) Pressure distribution in the meridian planes of a tube of outer radius $22L^*/9$ and inner radius $4L^*/9$ at Time Step 5000. Total 360 degrees are divided into 110 meshes, giving the azimuthal angle interval 3.36 degrees. Total grids are $450 \times 21 \times 110$, based upon the uniform grid spacing $L^*/9$. $K = 18 - 33$.

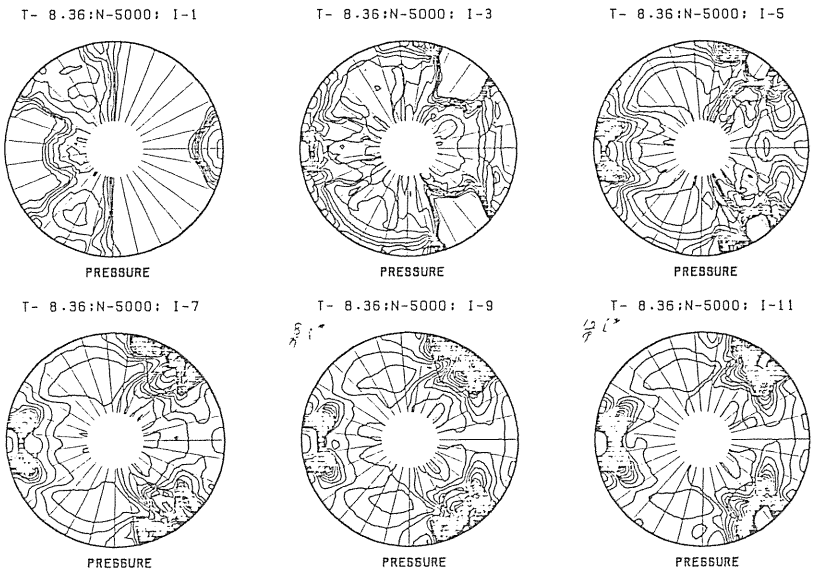

Fig. 4 (b) Pressure distributions in the cross sections of a tube of outer radius $22L^*/9$ and inner radius $4L^*/9$ at Time Step 5000; $I = 1 - 11$, corresponding to $z = (I-1)L^*/9$.

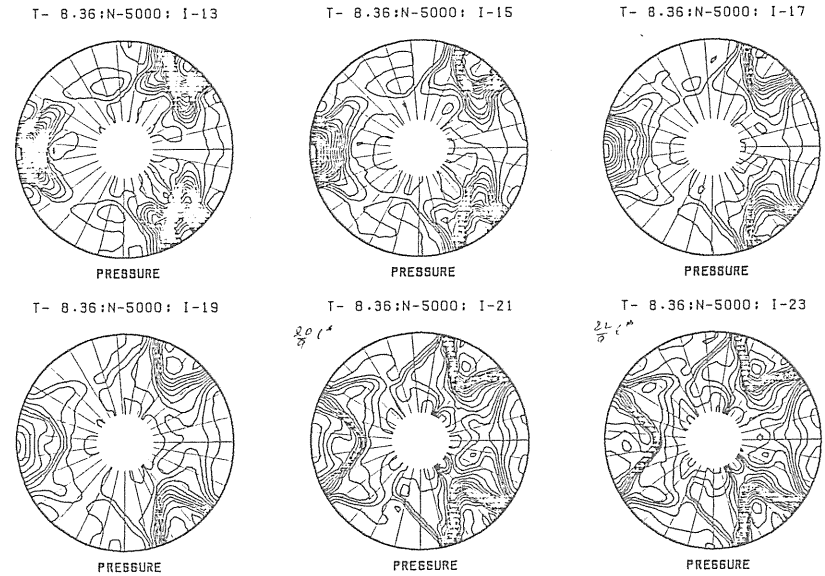

Fig. 4 (c) Pressure distributions in the cross sections of a tube of outer radius $22L^*/9$ and inner radius $4L^*/9$ at Time Step 5000; $I = 13 - 23$, corresponding to $z = (I-1)L^*/9$.

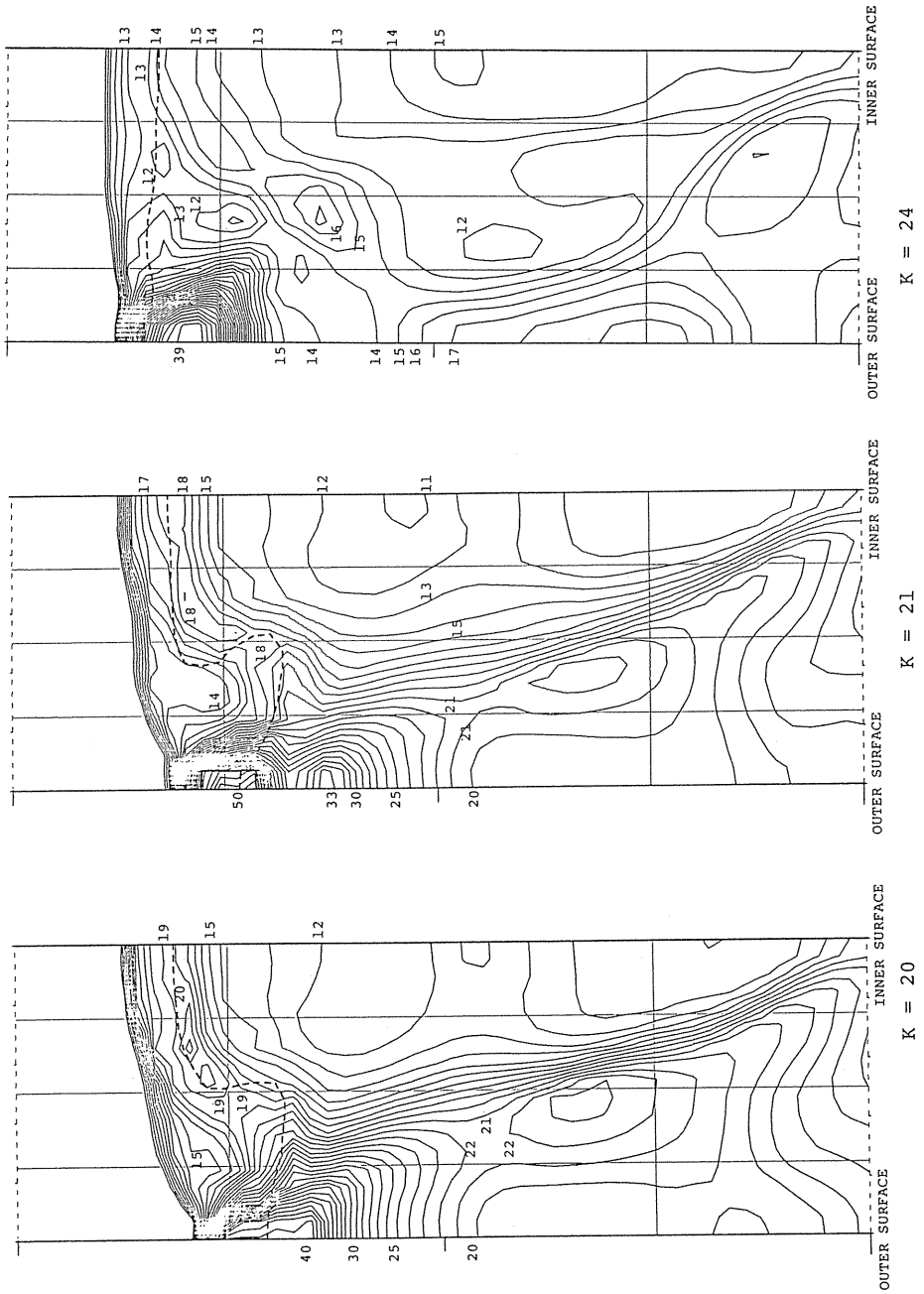

Fig. 4 (d) Close-ups of the pressure distributions in the meridian planes K = 20, 21 and 24. The numbers give the dimensionless value of each pressure contour with its spacing $\triangle p = 1.0$. The broken line is the locus of reaction front.

cross sections I = 1 − 23 in Figs. 4 (b) and (c); the shape is extremely skewed. Triple-shock structures are clearly seen in the meridian planes, for example, K = 18 − 25, where the existence of locally dense pressure contours characterizes the blast wave phenomena. In contrast, the meridian planes K = 26 − 33 give the flat frontal shock with the nearly one-dimensional downstream flow, as ssen in Fig. 4 (a).

If we observe, for example, the pressure contours in the tube cross section I = 1 and 3 in Fig. 4 (b), the roughness of the frontal shock wave is of the order of $\frac{2L^*}{9}$ where three azimuthally flapping waves are converging into the three concave portions in the frontal shock waves. As seen in I = 5 − 23 in Figs. 4 (b) and (c), such flapping waves have long tails extending to the downstream and, in addition, reflections from the outer wall. In contrast, the inner wall seems to play no essential roles, as was initially intended in the calculation.

Close-up pressure distributions in three successive meridian planes K = 20, 21 and 24 in Fig. 4 (a) are shown in Fig. 4 (d). One essential and interesting difference between two- and three-dimensional detonations we can notice in Fig. 4 (d) is that a location near the outer surface has already started explosion and yet the corresponding portion of the frontal shock wave has not been accelerated to bring it ahead of the remaining portion. If the explosion is of two-dimensional form, such a shape is quite unlikely. It can happen only in a three-dimensional phenomenon where a spherical blast wave is much weaker to influence the environment than a cylindrical one. The maximum pressure realized in the explosion reaches 50 (K = 21), which is much higher than the two-dimensional Neumann spike about 20.

4. 5. Pressure Distributions at Time Step N = 6,000:

When the previous calculation for Small Tube is extended to N = 6,000, the behaviors are seen in a number of coordinate meridian and cross-sectional planes, as shown in Figs. 5 (a)–(d). Figs. 5 (a) and (b) give a triple shock intersection propagating radially from the outer wall to inner one where the downstream portion has already reached the inner wall with an extremely shallow reflection angle. The detailed structure of a complex of triple shocks, highest-pressure plateau (43), expansion wave and reaction front is clearly observed in Fig. 5 (b). Generally speaking, the frontal shock wave is more skewed at this time step, as seen in Figs. 5 (c) and (d).

4. 6. Cross-Sectional Pressure Distributions in Large Tube:

Unlike the previous results, Figs. 6 (a) and (b) give the structure of a detonation propagating in Large Tube the outer and inner radii of which are $\frac{46L^*}{9}$, and $\frac{10L^*}{9}$ at Time Step N = 7,000. As seen in Fig. 6 (a), I = 1 − 3, the roughness of the frontal shock wave is of the order of $\frac{4L^*}{9}$ which is twice as large as in Small Tube. We can also observe, in Fig. 6 (a) I = 1 and 2, five pairs of flapping waves colliding each other. Compared with a detonation in Small Tube, the one in Large Tube shows more symmetry with respect to the relative location and ineraction of the flapping waves.

The increase from 3 in Small Tube to 5 in Large Tube of the number of flapping waves seems to confirm that for a given chemical system the number is an eigen value to the tube size (radius or thickness of a tube):

Tube Thickness in L^* (outer-inner radius)	Number of Flapping Waves
2	3
4	5

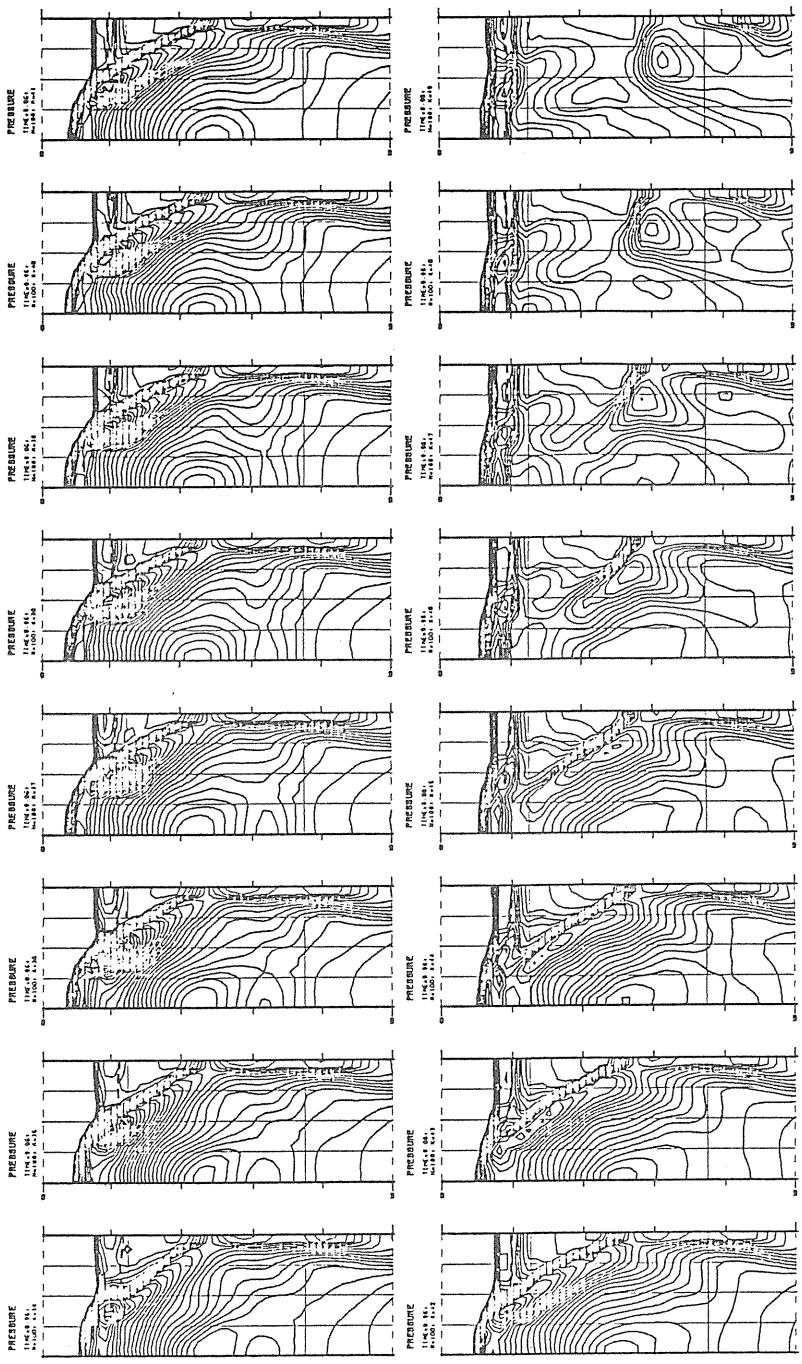

Fig. 5 (a) Pressure distribution in the meridian planes K = 34 – 49 of a tube of outer radius 22L*/9 and inner radius 4L*/9 at Time Step 6000.

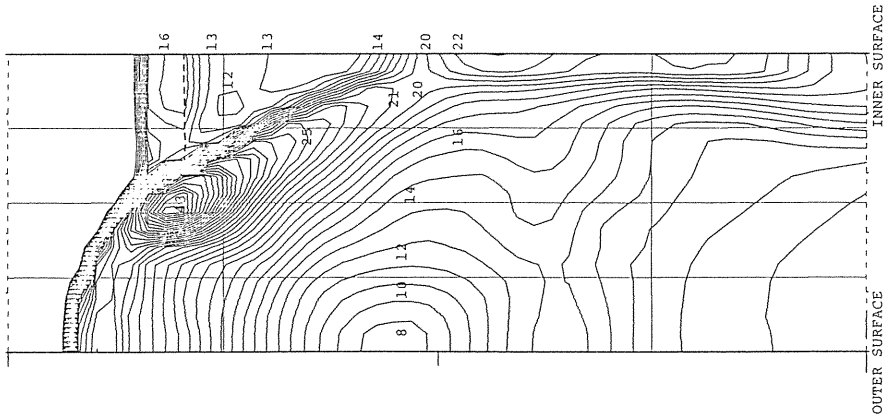

Fig. 5 (b) Close-up of the pressure distribution in the meridian plane K = 38. The number gives the dimensionless value of each pressure contour with its spacing $\Delta p = 1.0$. The broken line is the locus of reaction front.

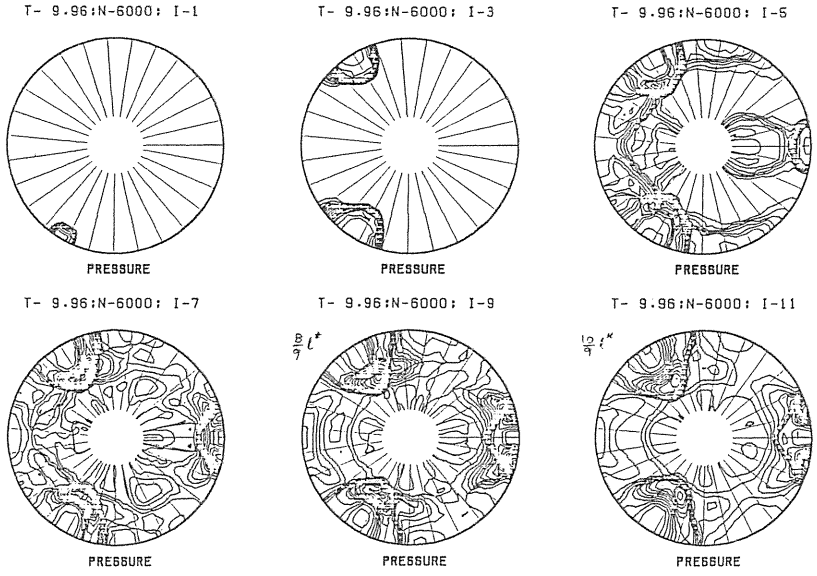

Fig. 5 (c) Pressure distributions in the cross sections of a tube of outer radius $22L^*/9$ and inner radius $4L^*/9$ at Time Step 6000; the cross sections $I = 1 - 11$, corresponding to $z = (I - 1)L^*/9$.

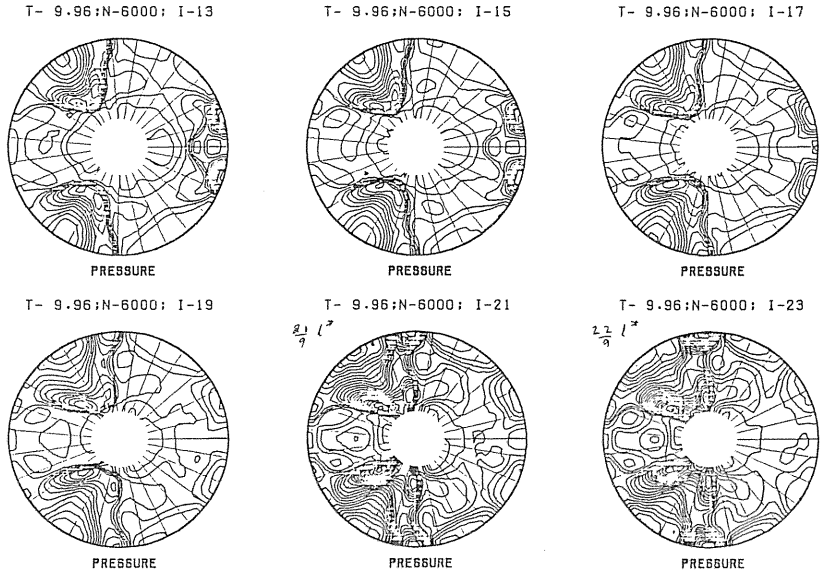

Fig. 5 (d) Pressure distributions in the cross sections of a tube of outer radius $22L^*/9$ and inner radius $4L^*/9$ at Time Step 6000; the cross sections $I = 13 - 23$, corresponding to $z = (I - 1)L^*/9$.

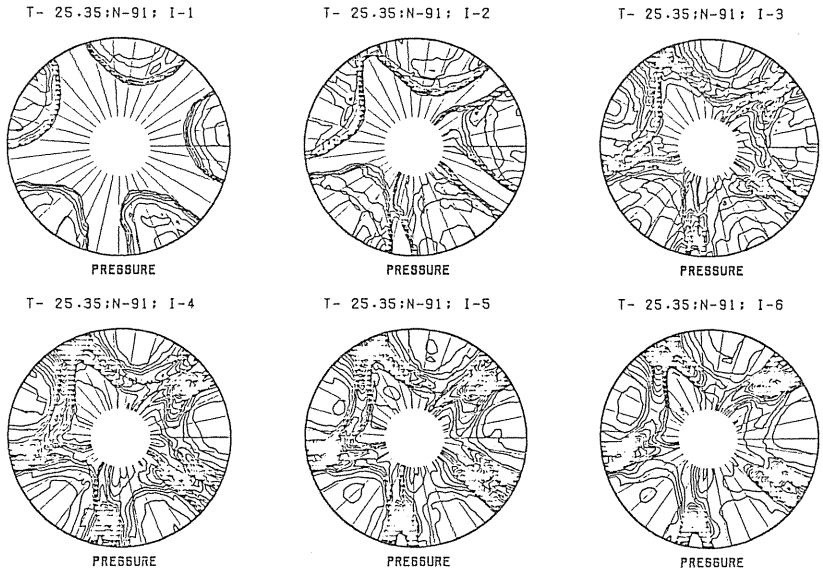

Fig. 6 (a) Pressure distributions in the cross sections $I = 1 - 6$ of a tube of outer radius $46L^*/9$ and inner radius $10L^*/9$ at Time Step 7000. Total 360 degrees are divided into 126 meshes, giving the azimuthal angle interval 2.927 degrees. Total grids are $350 \times 20 \times 126$, based upon the uniform grid spacing $2L^*/9$.

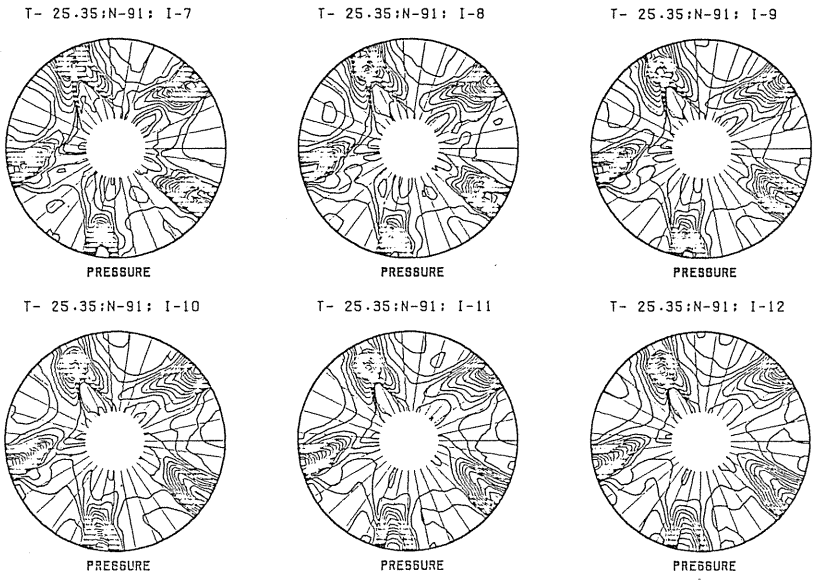

Fig. 6 (b) Pressure distributions in the cross sections I = 7 – 12 of a tube of outer radius 46L*/9 and inner radius 10L*/9 at Time Step 7000.

4. 7. Conclusions:

Based on the Euler equations, a three-dimensional detonation propagating in a circular cylinder is numerically solved, using the numerical scheme MacCormack-FCT that has been successfully applied to a number of two-dimensional problems. As was already proven in the numerical analysis of two-dimensional nonsteady detonations elsewhere by the author, the mechanism of self-sustenance of detonation is again the interaction among shock waves. The interaction, however, is three-dimensional, i.e. among three different modes propagating in axial, radial and azimuthal directions. Therefore observed are the complicated interaction among numerous physical phenomena like multiple-Mach-reflection of shock waves, nearly-point exothermic chemical explosion in the vicinity of a triple point, spherical blast waves and expansion waves, non-flat geometry of frontal shock wave, and the existence of three shock wave modes.

Of particular interest is the discovery of paired flapping shock waves propagating in the azimuthal direction. Although a "single-spin" detonation has not been observed in the present set of parameters, it seems to be a limiting condition where only one single azimuthal shock wave propagates instead of 3 or 5 paired ones seen in the present numerical calculations.